Recent cooling in the lower Pacific Ocean based on dynamically-consistent ocean syntheses

Fanglou Liao (fanglou.liao@unswalumni.com)
King Abdullah University of Science and Technology https://orcid.org/0000-0003-4843-4329
Peng Zhan
Department of Ocean Science and Engineering, Southern University of Science and Technology, Shenzhen
Xiao Hua Wang
The Sino-Australian Research Consortium for Coastal Management, School of Science, The University of New South Wales, Canberra, Australia
Zhiqiang Liu
Department of Ocean Science and Engineering, Southern University of Science and Technology, Shenzhen
Ibrahim Hoteit
KAUST

Article

Keywords:

Posted Date: April 27th, 2022

DOI: https://doi.org/10.21203/rs.3.rs-1599666/v1

Recent cooling in the lower Pacific Ocean based on dynamically-consistent ocean syntheses

Fanglou Liao[*1,2], Peng Zhan [2], Xiao Hua Wang [3], Zhiqiang Liu [4,5], and Ibrahim Hoteit [2].

[1] *Department of Ocean Science, Hong Kong University of Science and Technology, Hong Kong, China*

[2] *Division of Physical Sciences and Engineering, King Abdullah University of Science and Technology, Thuwal, Saudi Arabia*

[3] *The Sino-Australian Research Consortium for Coastal Management, School of Science, The University of New South Wales, Canberra, Australia*

[4] *Department of Ocean Science and Engineering, Southern University of Science and Technology, Shenzhen, China*

[5] *Southern Marine Science and Engineering Guangdong Laboratory (Guangzhou), Guangzhou, China*

Corresponding author: Fanglou Liao, fanglou.liao@unswalumni.com

ABSTRACT

The thermal state from 1993–2017 in the lower Pacific Ocean (below 2 km) was investigated using two dynamically-consistent syntheses. We show a robust and bottom-intensified cooling. This Pacific cooling is mainly determined by the meridional heat exchange with the Southern Ocean and the vertical heat advection. The abyssal Pacific Ocean loses heat by way of westward heat advection in the northwest ocean. Mixing is found to play a negligible role. This study is to some extent consistent with a recent study that presented a deep Pacific cooling as an adjustment to the last Little Ice Age. However, it contradicts with most recent studies, which argued the abyssal Pacific Ocean was warming over the recent two decades. Our study suggests that special caution is needed when auditing variations in the deep ocean and more work is in need for a better understanding of the deep ocean state.

1. Introduction

Estimating the ocean heat content (OHC) is essential to addressing the climate change. To date most OHC-related studies have been confined to the upper 2 km (Hakkinen et al. 2016; Levitus et al. 2012; Liang et al., 2021), as have most ocean measurements (Zilberman et al. 2020).

Previous studies, however, evidenced the importance of the deep ocean in the global heat storage (Palmer et al., 2011; Balmaseda et al., 2013; Cheng et al., 2016).

As the largest and deepest basin, and also where El Niño-Southern Oscillation (ENSO), a recurring climate pattern of global impact, occurs every 2 to 7 years over the tropical Pacific Ocean, the Pacific Ocean plays a vital role in the global climate (England et al., 2014). According to Wunsch and Heimbach (2014), the deep Pacific Ocean has the longest memory time, implying 'meteorological forcing of decades to thousands of years ago should still be producing trend like changes in abyssal heat content'.

A recent study by Gebbie and Huybers (2019) claimed that the deep Pacific Ocean (below 2 km) was still cooling as an ongoing response to the last Little Ice Age. This cooling, is possible, even in the context of global warming, given that the deep Pacific Ocean may respond to surface forcing at a much longer timescale than that of the forcing itself. In addition, interpretation of the global warming often relies on the assumption that ocean-atmosphere system is in equilibrium, with fluctuations arising directly from the recent decades (Liang et al. 2015). This deep Pacific cooling, however, contradicted with most recent studies on the thermal state change in deep Pacific Ocean, as briefly introduced as follows.

Purkey and Johnson (2010) estimated a heat flux of 0.027 (±0.009) $W \cdot m^{-2}$ into the global abyssal ocean during the 1990s and 2000s, indicating a statically significant warming trend intensified in the southernmost basins and weakened to the north. For the period from the 1990s to 2000s, Kouketsu et al. (2012) estimated that the global OHC below 3 km increased at a rate of 0.8×10^{22} J (J: Joule) per decade. With updated datasets, Desbruyeres et al. (2016) extended the work of Purkey and Johnson (2010) and reproduced a warming trend below 2 km, particularly between 4–6 km. Later, Desbruyeres et al. (2017) obtained mostly similar results to Desbruyeres et al. (2016), but the warming trend of the deep Pacific Ocean (2–4 km) in Desbruyeres et al. (2016) reversed into a cooling in Desbruyeres et al. (2017), noting that the two have an overlapping temporal window. The abyssal Pacific warming is consistent in these two consecutive studies. Warming in the abyssal Pacific Ocean was also shown in Durack et al. (2018) and Johnson et al. (2019). Overall, these above-mentioned studies revealed a possible warming in the abyssal Pacific Ocean over the recent decades and the results in the deep Pacific Ocean (2–4 km) are more mixed. These mixed findings may be to some extent due to the different time periods considered in each study.

It is virtually certain that the revealed warming trend in the abyssal Pacific Ocean (and may be also the deep Pacific Ocean) is both interesting and of significant importance. However, one may need to be cautious in interpreting these trends. This is mainly because results derived from the repeat hydrographic measurements were based on some simplifications. For example, the previous studies generally took data along a few or even one single hydrographic section to represent a whole sub-basin and the occupation time of different sections was different and short. These spatially and temporally sparse datasets may inevitably lead to uncertainties in estimating the state variations of the lower Pacific Ocean.

There is therefore a need to revisit this scientific question using state-of-the-art datasets of a much higher density in both temporal and spatial domains. An oceanic synthesis assimilating most available measurements suits for this aim. Among the many products, ECCOv4r4 (version 4, release 4 of Estimating the Circulation and Climate of the Ocean (Forget et al. 2015)) and GECCO3 (version 3 of German contribution to the Estimating the Circulation and Climate of the Ocean project (Köhl 2020)) stand out as dynamically consistent ocean state estimates. Although models may suffer from drifts and the unwanted trends induced by the changing observations assimilated, the single assimilation window used in ECCOv4r4 and GECCO3 can significantly reduce these uncertainties.

Here, we use ECCOv4r4 (ECCO) and GECCO3 (GECCO) to examine the warming/cooling in the lower Pacific Ocean below 2 km in 1993–2017. Using two datasets helps to examine the sensitivity to the model resolution, forcing, assimilated observations and integration period. Results based on GECCO are presented as supplementary materials, but are frequently referred to in the text. The remainder of this manuscript is set out as follows. A brief description of the data and methods of analysis is in Methods section. Section 2 gives the temporal and spatial characteristics of the potential-temperature change and OHC, and also a heat-budget analysis. A discussion is given in section 3.

2. Results

a. Time evolution of OHC and meridional distribution of the linear OHC trend

Fig. 1a shows the bathymetry of the domain, similar to that in Desbruyères et al. (2017). Note that grids with depth shallower than 2 km are masked out. The region bounded by the black and red dashed lines are used for a later heat budget analysis (Section 3.4). South to the red dash line is recognized as the Southern Ocean, which experienced intense warming (Fig. 3).

The choice of the boundaries (red and black dash lines) is clearly somewhat arbitrary, but is reasonable and convenient for the heat budget analysis.

It is evident that both the deep and abyssal Pacific Oceans experienced an approximately linear cooling from 1993 to 2017 (Fig. 1). The OHC decreased at $4.4\pm0.4\times10^{20}$J·yr^{-1} in the deep ocean and $3.4\pm0.8\times10^{20}$J·yr^{-1} in the abyssal ocean. The uncertainty (shading) was small. This linear decreasing trend of OHC is robust in both datasets (Figs. 1 and S1) and similar to the results in Gebbie and Huybers (2019) in the overlapping period.

Besides, we calculated the linear trend of OHC as a function of latitude and we considered three periods: from 1993 to 2005 (Fig. 1c), from 2006 to 2017 (Fig. 1d) and from 1993 to 2017 (Fig. 1e) , similar to Desbruyères et al. (2016). South to around 30°S, the Pacific Ocean below 2 km largely warmed and the warming between 2–4 km accelerated during 2006–2017, associated with the recent warming in the Southern Ocean (Sallée 2018). North to around 30°S, both the deep and abyssal Pacific Oceans cooled in all the three different periods. The deep cooling was strongest equatorward of 20°; the strongest abyssal cooling occurred at around 27°N. North to 40°N, the trend was weak in the abyssal ocean from ECCO. Below 4 km, there are no notable differences occurring with time in both the two datasets. The GECCO results were similar to those from ECCO, further increasing our confidence in the cooling trend.

Fig. 1.

b. Vertical distribution of the potential temperature change

Some detail was lost in taking layer (vertical) averages in section 3.1. In this section, we considered the horizontal-averaged potential temperature and its linear trend.

Below 2 km, cooling occurred at almost all the vertical levels, with bottom intensification seen in both ECCO (Fig. 2) and GECCO (Fig. S3). The temperature decreased by about 0.05°C near the bottom but less than 0.01°C at around 2 km. Cooling between 2.3–3.5 km accelerated from around 2011. The vertical profile quantitatively shows an approximate cooling rate of 2.3×10^{-3} °C·yr^{-1} near the bottom but slower than 0.5×10^{-3} °C·yr^{-1} near 2 km. The cooling rate was vertically homogeneous in the deep Pacific Ocean between 2–4 km. Fig. 2b shows that the cooling above 5 km slowed down in 2006–2017 when comparing to 1993–2005, but is almost time-invariant further below. Similarly, GECCO also presents statistically significant cooling in the Pacific Ocean below 2 km (Fig. S3), suggestive of robust Pacific cooling below 2 km.

123 The strongest cooling rate near the bottom is of comparable magnitude in these two ocean
124 syntheses. However, the GECCO cooling trend was less vertically homogeneous between 2–4
125 km. Below 4 km, GECCO generally estimated a more intense cooling than ECCO. In addition,
126 the GECCO reveals a recent cooling slowdown except between 3–4 km.

127 Fig. 2.

128 *c. Geographic pattern of potential temperature change*

129 A detailed geographic distribution helps to better understand where cooling occurs and its
130 spatial heterogeneity. Figs. 3 and S4 presented a trend map of the vertically-averaged potential
131 temperature.

132 Intense warming patches appeared in the southernmost basin, consistent with the finding of
133 previous studies (e.g., Desbruyères et al. 2017; Volkov et al., 2016). Specifically, there was
134 strong warming in both the southwest and southeast regions. The southwest waring is
135 associated with the northward Lower Circumpolar Deep Water (LCDW) inflow along the
136 eastern edge of New Zealand (Kawabe and Fujio, 2010), intensified during 2006–2017. This
137 warming between 2–4 km largely result from the horizontal convergence of heat flux (Fig. S5)
138 but was mainly attributed to the geothermal flux in the abyssal ocean (Fig. S6). In the northwest
139 deep ocean, ECCO showed a warming trend that decreased in intensity from a moderate level
140 in 1993–2005 to be negligible over the 25-year period. The vertical convergence determined
141 this warming (Fig. S5), probably meaning that water was cooling in the formation of Pacific
142 Deep Water (PDW) via upwelling. However, cooling clearly dominated over most of the area,
143 and was particularly strong west of North America, one of the regions with the longest memory
144 time (Wunsch and Heimbach 2014). Therefore, this cooling patch is at least physically
145 plausible as it takes quite a long time for this region to response to the currently experiencing
146 warming imposed by the increasing greenhouse gas concentrations. This area is a hotspot of
147 strong horizontal and vertical heat flux of opposite signs (Fig. S5), with the horizontal (vertical)
148 one dominates in the deep (abyssal) ocean. The intense horizontal divergent heat flux is likely
149 a result of the southward flow of north PDW, which then mixes with the Upper Circumpolar
150 Deep Water (UCDW) and returns to the Southern Ocean (Kawabe and Fujio, 2010; Ma et al.,
151 2018). The abyssal horizontal convergence of heat flux may infer eastward flow of LCDW.
152 This intense cooling weakened over time, likely occurred between 4–5 km from Fig. 2. In
153 general, the widespread cooling in the deep and abyssal Pacific Oceans is largely determined
154 by the horizontal and vertical convergent/divergent heat flux, with heating from the vertical

diffusion and geothermal flux, the latter especially strong along the East Pacific Rise (Figs. S5–6).

The overall pattern was largely the same from GECCO (Fig. S4). To some extent, the deep northwest warming pattern agrees with the warming along 137°E in Tian et al. (2020), but they showed warming penetrated as deep as 5 km. Again, cooling was the predominant pattern. However, the warming in the southeast deep Pacific Ocean was weaker in the GECCO. In addition, the intense cooling (2–4 km) west to the north American continent in ECCO was invisible in GECCO. Moreover, GECCO presented a zonal-band of warming in the northern tropics of the deep Pacific Ocean. The strongest abyssal cooling was geographically close, but the intensity was lower in GECCO. Johnson et al. (2019) showed the southwest Pacific experienced statistically significant warming below 4900 dbar but cooling between 2100 and 4300 dbar. Our results below around 4 km in this region is different, possibly due to different time periods. The widespread cooling found here is similar to Gebbie and Huybers (2019), but again the time periods were different.

Besides, we decomposed the potential temperature variations into heave (HV) and spice (SP) components following Bindoff and McDougall (1994), shown in Fig. S7. HV stands for the potential temperature change due to vertical displacement of neutral density surface and the SP represents the potential temperature change along the neutral density surface (Häkkinen et al., 2016). South to 20°S, both ECCO and GECCO reveal strong HV-related warming. SP-related warming is also notable in the Southern Ocean from ECCO but not GECCO, probably implying their differences in the salinity simulation. North to 20°S, cooling dominates, with only water occupying density range 27.9–28.1($kg \cdot m^{-3}$) warms north to 20°N. This corresponds to the northwest Pacific SP-related warming, implying salination via density compensation. The most intense cooling in the north Pacific Ocean results from both HV and SP cooling, and is most likely related to the LCDW (28.1 $kg \cdot m^{-3}$ (Talley (2011)).

Fig. 3.

d. Heat budget analysis

To determine the major contributors to cooling, we performed a heat budget analysis based on ECCO (Fig. 4), within the box bounded by the red and black dashed lines in Fig. 1a. Neither the northern side (Bering Strait, shallower than 2 km) nor the eastern side (landmass) of the domain contributed to the OHC variations below 2 km. Advection and diffusion of heat were

186 calculated following Equation (1). The geothermal heat flux was included at the bottom grid.
187 Publicly available outputs from GECCO are not sufficient to close the budget, and thus no
188 efforts were taken to achieve a heat budget analysis using GECCO. It is worthy to note,
189 however, that heat budget is closed in the dynamically-consistent GECCO.

190 Clearly, the heat diffusion was much weaker than the advection (Fig. 4). The two primary
191 processes were the meridional heat advection through the southern boundary and the vertical
192 heat advection. The former transported heat into the domain above about 3 km and out at
193 greater depths, indicating a meridional overturning structure. The zonal advection through the
194 western boundary and the geothermal flux generally played only a moderate role. However,
195 near 6 km, the abyssal cooling largely came from the westward heat flux through the western
196 boundary.

197 The deep ocean lost heat through the southern boundary at 2–3.5 km (3.5 km is approximately
198 the depth of the neutral density of 28.16 $kg \cdot m^{-3}$ in Kouketsu et al. (2011)) but the vertical heat
199 advection accumulated heat at 2–3 km: the heat loss was stronger, so cooling occurred. Below
200 about 3km, the deep ocean lost heat vertically (formation of PDW) but was heated through the
201 southern boundary below 3.5km (northward transport by LCDW); the vertical heat loss was
202 again much stronger. Given the volume conservation, this implies the temperature difference
203 between water within the deep Pacific Ocean and water from the Southern Ocean.

204 The meridional heat advection was closely linked to the deep Pacific meridional overturning,
205 with northward transport of major bottom water (LCDW) confined to the western ocean
206 (Kouketsu et al., 2011), mainly along the east of New Zealand. Previous studies (e.g., Kouketsu
207 et al., 2011; Voet et al., 2016) explained their findings of deep and abyssal Pacific warming as
208 a result of the slowdown of the northward volume transport. Our calculations of the northward
209 volume flux showed a similar decreasing trend in the recent years (Fig. S8) but contradict the
210 conclusion that this reduced transport led to deep and/or abyssal warming. The differences
211 between ECCO and GECCO in the calculated volume flux and cooling patterns, however, may
212 reflect the sensitivity of the temperature in the deep and abyssal ocean to the flow of major
213 bottom water.

214 Fig. 4.
215
216

3. Discussion

The most surprising result is the intense cooling in the abyssal Pacific Ocean, inconsistent with most of the previous investigations. The primary difference lies in the nature of the data used, sparse hydrographic measurements in previous studies, while dynamically-consistent ocean syntheses in this study. Our work here provides further evidence of the deep Pacific cooling, and calls into question the widely debated abyssal Pacific warming.

The cooling of the abyssal Pacific Ocean shown here is of considerable climate significance. The Pacific Ocean has the largest volume of all the oceans, and the oceans are important heat buffers in the changing climate system. That is, if the lower part of the ocean cools, less heat it absorbed and more heat advected upward into the upper part of the ocean, seen from our heat budget analysis. A heavier heat-intake burden will therefore be imposed on the upper ocean. Moreover, if this cooling continues, it may lead to an increasingly stronger stratification at the interface (e.g., 2 km) between the lower and upper ocean. This barrier will further restrict the heat absorbed by the abyssal ocean and impact the upper circulation (Peng et al., 2022).

ECCO and GECCO complemented each other in several ways. First, they had different atmospheric forcing, suggesting that differences in atmospheric forcing are not a determining factor in the warming/cooling trend in the lower Pacific Ocean. Second, GECCO had a much longer integration period than ECCO, indicating the robustness of current findings with respect to the assimilation window used in these two products. In fact, GECCO indicates that both the lower Pacific cooling persist since 1948 (the first year of GECCO integration), although the cooling rate decreases in most recent decades (not shown). Third, the assimilated datasets are different. Last, the grid spacing was different: ECCO has denser vertical grids but sparser horizontal grids.

Besides, we also analyzed other datasets including both eddy-permitting and eddy-resolving ones (not shown), such as Ocean General Circulation Model For the Earth Simulator (OFES (Masumoto et al. 2004; Sasaki et al., 2004)) and Bluelink ReANalysis (BRAN), version 2020 (Chamberlain et al. 2021), and among others. It was found that dynamically-consistent models (e.g., OFES) generally indicate cooling in the lower Pacific Ocean and dynamically-inconsistent models (BRAN2020) are more likely to present a warming trend. Some global eddy-resolving reanalysis (e.g., BRAN2020 and GLORYS12V1 (Jean-Michel et al. 2021)) present a cooling trend before around the middle of 2000s and strong warming from the middle

of 2000s to the end of 2010s. This may be due to an intrinsic characteristics of the traditional sequential assimilation strategy, which is sensitive to the volume of observations assimilated, knowing that there is a major transition of the observation platform from ship-based ones to the Argo floats in the middle of 2000s (Abraham et al., 2013; Cheng et al., 2014). Although Argo floats (except the Deep Argo project) are confined to the top 2 km, it is possible that artefacts induced by this observation transition in the top 2 km leads to noticeable changes in the lower ocean. Furthermore, we compared four SODA3 (Carton et al., 2018) reanalysis and their corresponding unconstrained simulations. The only difference between a SODA3 reanalysis and its simulation counterpart is that the reanalysis assimilates observations. It is evident that all observation-constrained SODA3 reanalysis (dynamically-inconsistent) have a marked warming bias relative to the unconstrained SODA3 simulation, which shows a weak cooling between around 2–4 km and a weak warming or cooling beneath.

Garry et al. (2019) constructed a framework to examine the bias induced by the temporally-spatially sparse observational-style sampling. They applied this novel framework to an ocean model and argued that around 80% of global deep warming can be represented by the observational-style sampling in the model. In the meantime, the authors acknowledged that this conclusion only depends on one single simulation. Indeed, a recent work based on ECCO suggested that this observational-style sampling works between 2–4 km but may substantially underestimate the cooling trend below 4 km in the Pacific Ocean (personal communication with Y. Zhang, April 2022). This is consistent with our study that model-derived trends are similar and in contrast to observation-based results in the deep and abyssal Pacific Oceans, respectively.

Although our study is to some extent consistent with Gebbie and Huybers (2019), one should note that the temporal length considered in this study is much shorter. With that said, results covering the 71-yrs period using GECCO indicates that the Pacific adjustment to the last Little Ice Age may still persist. Results and conclusions reported in this manuscript, however, are not intended to and cannot rule out the possibility of warming in the lower Pacific Ocean as found in prior studies, as both models and observations have drifts or biases. Therefore, the realistic situation may be a compromise between the calculated trends in our study and prior ones. We expect improvements in both observations (e.g., Deep Argo program) and models (e.g., a higher resolution and better mixing parameterization) to enhance our understanding of the deep ocean state.

Acknowledgments. We thank the ECCO and GECCO teams for the publicly available datasets. Dr. Peter McIntyre helped to improve the manuscript. An earlier version of this manuscript was commented by Dr. Jiping Xie. We are also grateful for Hong Zhang from the Jet Propulsion Laboratory in helping with the heat budget analysis and Yang Zhang from University of Delaware for providing information about potential bias of using sparse observations in auditing the abyssal warming/cooling in the Pacific Ocean.

Author contributions. F.L. conceived the study. F.L. and P.Z. framed the structure. F.L. conducted the calculations and drafted the manuscript. F.L. and P.Z. leaded the result analysis. All authors discussed the results and contributed to improving the manuscript.

Data Availability. The ECCOv4r4 data can be access from https://www.ecco-group.org/products-ECCO-V4r4.htm; GECCO3 data is available at https://www.cen.uni-hamburg.de/en/icdc/data/ocean/reanalysis-ocean/gecco3.html.

Code availability. Codes to reproduce this study is available from F.L. on request.

Competing interests. The authors declare no competing interests.

REFERENCES

Abraham, J. P., and Coauthors, 2013: A review of global ocean temperature observations: Implications for ocean heat content estimates and climate change. *Rev. Geophys.*, **51**, 450–483, https://doi.org/10.1002/rog.20022.

Balmaseda, M., K. E. Trenberth, and E. Erland Källén, 2013: Distinctive climate signals in reanalysis of global ocean heat content. *Geophys. Res. Lett.*, **40**(9), 1754–1759. https://doi.org/10.1002/grl.50382.

Carton, J. A., G. A. Chepurin, and L. Chen, 2018: SODA3: A new ocean climate reanalysis. *J. Clim.*, **31**, 6967–6983, https://doi.org/10.1175/JCLI-D-18-0149.1

Chamberlain, M. A., P. R. Oke, R. A. S. Fiedler, H. M. Beggs, G. B. Brassington, and P. Divakaran, 2021: Next generation of Bluelink ocean reanalysis with multiscale data assimilation: BRAN2020. *Earth Syst. Sci. Data.*, *13*, 5663–5688, https://doi.org/10.5194/essd-13-5663-2021.

Cheng, L., and J. Zhu, 2014: Artifacts in variations of ocean heat content induced by the observation system changes. *Geophys. Res. Lett.*, **41**, 7276–7283, https://doi.org/10.1002/2014GL061881.

Cheng, L., K. E. Trenberth, M. D. Palmer, J. Zhu, and J. P. Abraham, 2016: Observed and simulated full-depth ocean heat content changes for 1970–2005. *Ocean Sci.*, **12**, 925–935, https://doi.org/10.5194/os-12-925-2016.

Dee, D. P., and Coauthors, 2011: The ERA-Interim reanalysis: configuration and performance of the data assimilation system. *Q. J. R. Meteorol. Soc.*, **137**, 553–597, https://doi.org/10.1002/qj.828.

Desbruyeres, D., S. G. Purkey, E. L. Mcdonagh, G. C. Johnson, and B. A. King, 2016: Deep and abyssal ocean warming from 35 years of repeat hydrography. *Geophys. Res. Lett.*, **43**(19), 10356–10365, https://doi.org/10.1002/2016GL070413.

Desbruyères, D., E. L. McDonagh, B. A. King, and V. Thierry, 2017: Global and Full-Depth Ocean Temperature Trends during the Early Twenty-First Century from Argo and Repeat Hydrography. *J. Clim.*, **30**(6), 1985–1997, https://doi.org/10.1175/JCLI-D-16-0396.1

Durack, P. J., P. J. Gleckler, S. G. Purkey, G. C. Johnson, J. M. Lyman, and T. P. Boyer, 2018: Ocean warming: From the surface to the deep in observations and models. *Oceanography*, **31**(2), 41–51, https://doi.org/10.5670/oceanog.2018.227.

ECCO Consortium, I. Fukumori, O. Wang, I. Fenty, G. Forget, P. Heimbach, and R. M. Ponte, 2020: ECCO Central Estimate (Version 4 Release 4). Retrieved from https://ecco.jpl.nasa.gov/drive/files/Version4/Release4.

England, M. H., and Coauthors, 2014: Recent intensification of wind-driven circulation in the Pacific and the ongoing warming hiatus. *Nat. Clim. Change*., **4**, 222–227, https://doi.org/10.1038/nclimate2106.

Forget, G., J. Campin, P. Heimbach, C. N. Hill, R. M. Ponte, and C. Wunsch, 2015: ECCO version 4: an integrated framework for non-linear inverse modeling and global ocean state estimation. *Geosci. Model Dev*., **8**, 3071–3104, https://doi.org/10.5194/gmd-8-3071-2015.

Forget, G., and D. Ferreira, 2019. Global ocean heat transport dominated by heat export from the tropical Pacific. *Nat. Geosci*., **12**, 351–354, https://doi.org/10.1038/s41561-019-0333-7.

Garry, F. K., E. L. McDonagh, A. T. Blaker, C. D. Roberts, D. G. Desbruyères, E. Frajka-Williams, and B. A. King, 2019: Model-Derived Uncertainties in Deep Ocean Temperature Trends Between 1990 and 2010. *J. Geophys. Res. Oceans*., **124**, 1155–1169, https://doi.org/10.1029/2018JC014225.

Gaspar, P., Y. Grégoris, and J.-M. Lefevre, 1990: A simple eddy kinetic energy model for simulations of the oceanic vertical mixing: Tests at station Papa and long-term upper ocean study site. *J. Geophys. Res. Oceans*., **95**(C9), 16179–16193, https://doi.org/10.1029/JC095iC09p16179.

Gebbie, G., and P. Huybers, 2019: The Little Ice Age and 20th-century deep Pacific cooling. *Science*, **363**(6422), 70–74, https://doi.org/10.1126/science.aar8413.

Good, S. A., M. Martin, and N. A. Rayner, 2013: EN4: Quality controlled ocean temperature and salinity profiles and monthly objective analyses with uncertainty estimates. *J. Geophys. Res. Oceans*., **118**(12), 6704–6716, https://doi.org/10.1002/2013JC009067.

Hakkinen, S., P. B. Rhines, and D. L. Worthen, 2016: Warming of the Global Ocean: Spatial Structure and Water-Mass Trends. *J. Clim.*, **29**(13), 4949–4963, https://doi.org/10.1175/JCLI-D-15-0607.1.

Jean-Michel, L., and Coauthors, 2021: The Copernicus Global 1/12° Oceanic and Sea Ice GLORYS12 Reanalysis. *Front. Earth Sci.*, **9**, 698876, https://doi.org/10.3389/feart.2021.698876.

Johnson, G. C., S. G. Purkey, N. V. Zilberman, and D. Roemmich, 2019: Deep Argo Quantifies Bottom Water Warming Rates in the Southwest Pacific Basin. *Geophys. Res. Lett.*, **46**(5), 2662–2669, https://doi.org/10.1029/2018GL081685.

Kalnay, E., and Coauthors, 1996: The NCEP/NCAR 40-Year Reanalysis Project. *Bull. Am. Meteorol. Soc.*, **77**(3), 437–471, https://doi.org/10.1175/1520-0477(1996)077<0437:TNYRP>2.0.CO;2.

Kawabe, M., and S. Fujio, 2010: Pacific ocean circulation based on observation. *J. Oceanogr.*, **66**(3), 389–403, https://doi.org/10.1007/s10872-010-0034-8.

Köhl, A., 2020: Evaluating the GECCO3 1948–2018 ocean synthesis – a configuration for initializing the MPI-ESM climate model. *Q. J. R. Meteorol. Soc.*, **146**(730), 2250–2273, https://doi.org/10.1002/qj.3790.

Kouketsu,S., Doi, and Coauthors, 2011: Deep ocean heat content changes estimated from observation and reanalysis product and their influence on sea level change. *J. Geophys. Res. Oceans.*, **116**, C03012, https://doi.org/10.1029/2010JC006464.

Large, W., and S. Yeager, 2004: Diurnal to Decadal Global Forcing for Ocean and Sea-Ice Models: The Data Sets and Flux Climatologies. https://doi.org/10.5065/D6KK98Q6.

Lee, S., and Coauthors, 2015: Pacific origin of the abrupt increase in Indian Ocean heat content during the warming hiatus. *Nat. Geosci.*, **8**, 445–449, https://doi.org/10.1038/ngeo2438.

Levitus, S., and Coauthors, 2012. World ocean heat content and thermosteric sea level change (0–2000 m), 1955–2010. *Geophys. Res. Lett.*, **39**(10), L10603, https://doi.org/10.1029/2012GL051106.

Liang, X., C. Liu, R. M. Ponte, and D. P. Chambers, 2021: A Comparison of the Variability and Changes in Global Ocean Heat Content from Multiple Objective Analysis Products During the Argo Period. *J. Clim.*, **34**(19), 7875–7895, https://doi.org/10.1175/JCLI-D-20-0794.1.

Liang, X., C. Wunsch, P. Heimbach, and G. Forget, 2015: Vertical Redistribution of Oceanic Heat Content. *J. Clim.*, **28**(9), 3821–3833, https://doi.org/10.1175/JCLI-D-14-00550.1.

Ma, X., J. Tian, W. Ma, K. Li, and J. Yu, 2018 : Changes of deep Pacific overturning circulation and carbonate chemistry during middle Miocene East Antarctic ice sheet expansion. *Earth & Planet. Sci. Lett.*, **484**, 253–263, https://doi.org/10.1016/j.epsl.2017.12.002.

Masumoto, Y., and Coauthors, 2004: A fifty-year eddy-resolving simulation of the world ocean: Preliminary outcomes of OFES (OGCM for the Earth Simulator). *J. Earth Simulator*, **1**, 35–56, https://doi.org/10.32131/jes.1.35.

Palmer, M. D., D. J. Mcneall, and N. Dunstone, 2011: Importance of the deep ocean for estimating decadal changes in Earth's radiation balance. *Geophys. Res. Lett.*, **38**(13), L13707. https://doi.org/10.1029/2011GL047835.

Peng Q., and Coauthors, 2022: Surface warming–induced global acceleration of upper ocean currents. *Science Advances*, **8**, eabj8394, https://doi.org/10.1126/sciadv.abj8394.

Piecuch, C. G., 2017: A Note on Practical Evaluation of Budgets in ECCO Version 4 Release 3. 1–34.

Purkey, S., and G. Johnson, 2010. Warming of Global Abyssal and Deep Southern Ocean Waters Between the 1990s and 2000s: Contributions to Global Heat and Sea Level Rise Budgets. *J. Clim.*, **23**(23), 6336–6351, https://doi.org/10.1175/2010JCLI3682.1.

Redi, M. H., 1982: Oceanic Isopycnal Mixing by Coordinate Rotation. *J. Phys. Oceanogr.*, **12**(10), 1154–1158, https://doi.org/10.1175/1520-0485(1982)012<1154:OIMBCR>2.0.CO;2

Sallée, J.-B., 2018: Southern Ocean Warming. *Oceanography*, **31**, 52–62, https://doi.org/10.5670/oceanog.2018.215.

417 Sasaki, H., and Coauthors, 2004: A series of eddy-resolving ocean simulations in the world
418 ocean - OFES (OGCM for the Earth Simulator) project. Oceans '04 MTS/IEEE Techno-
419 Ocean '04 (IEEE Cat. No.04CH37600), 3, 1535-1541.

420 Tian, Z., and Coauthors, 2021: Water-Mass Properties and Circulation in the Deep and
421 Abyssal Philippine Sea. *J. Geophys. Res. Oceans*., **126**(6), e2020JC016994,
422 https://doi.org/10.1029/2020JC016994

423 Trenberth, K. E., J. T. Fasullo, K. Von Schuckmann, and L. Cheng, 2016: Insights into
424 Earth's Energy Imbalance from Multiple Sources. *J. Clim*., **29**(20), 7495–7505,
425 https://doi.org/10.1175/JCLI-D-16-0339.1.

426 Talley, L. D., 2011: *Descriptive physical oceanography: an introduction*. Academic press.

427 Trenberth, K. E., L. Cheng, P. Jacobs, Y. Zhang, and J. Fasullo, 2018: Hurricane Harvey
428 Links to Ocean Heat Content and Climate Change Adaptation. *Earth's Future*, **6**(5), 730–
429 744, https://doi.org/10.1029/2018EF000825.

430 Voet, G., and Coauthors, 2016. Warming and Weakening of the Abyssal Flow through
431 Samoan Passage. *J. Phys. Oceanogr*., **46**(8), 2389–2401, https://doi.org/10.1175/JPO-D-16-
432 0063.1.

433 Volkov, D. L., S.-K. Lee, F. W. Landerer, and R. Lumpkin, 2017: Decade-long deep-ocean
434 warming detected in the subtropical South Pacific. *Geophys. Res. Lett*., **44**(2), 927–936,
435 https://doi.org/10.1002/2016GL071661

436 Wunsch, C., and P. Heimbach, 2014: Bidecadal Thermal Changes in the Abyssal Ocean. *J.*
437 *Phys. Oceanogr*., **44**(8), 2013–2030, https://doi.org/10.1175/JPO-D-13-096.1.

438 Zilberman, N. V., D. H. Roemmich, and J., Gilson, 2020: Deep-Ocean Circulation in the
439 Southwest Pacific Ocean Interior: Estimates of the Mean Flow and Variability Using Deep
440 Argo Data. *Geophys. Res. Lett*., **47**(13), e2020GL088342,
441 https://doi.org/10.1029/2020GL088342.

442

443

Methods

ECCO and GECCO data. The ECCOv4r4 is the latest ECCO ocean state estimate product spanning from 1992 to 2017 (Forget et al., 2015; ECCO et al., 2020). It is based on the MIT general circulation model (MITgcm), with surface fluxes derived from 6-hourly atmospheric forcing from the ERA-Interim reanalysis fields (Dee et al. 2011) via bulk formulae of Large and Yeager (2004) and is constrained by nearly all modern ocean observations (ECCO et al., 2020). The ability to use information contained in those observations is achieved using a 4d-Var assimilation scheme, in which adjoint sensitivities provide a practical means to reduce spurious model drifts and biases, through inversion of uncertain model state variables. It maintains the dynamic balance of the model solution and avoids adding source/sink terms of unknown nature to the model equations over conventional sequential assimilation methods. The horizontal grid spacing is 1° zonally, and meridionally ranges from 0.25° near the Equator and poles to 1° at mid latitudes. There are 50 vertical levels, apart from 10 m at the surface and 457 m at 5900 m depth.

The GECCO3 is the first global dynamically-consistent and eddy-permitting synthesis spanning from 1948 to 2018 (Köhl 2020). It is based on the MITgcm, with atmospheric forcing from the 6-hourly NCEP RA1 reanalysis fields (Kalnay et al. 1996). The surface fluxes were derived following Large and Yeager (2004). The nominal horizontal resolution is 0.4° and there are 40 levels apart from 12 m at the surface to 600 m at depth (Köhl 2020). The assimilated temperature profiles are mainly from the EN4.2.1 (Good et al., 2013), an objective analysis of subsurface temperature and salinity at the Met Office Hadley Centre.

OHC and potential-temperature changes. In this study, we defined the deep ocean as depths 2–4 km, and the abyssal ocean as depths below 4 km. For each layer (deep or abyssal), we calculated time series of OHC by incorporating grid volume, seawater density, potential temperature and specific-heat capacity (Equation (1)). We excluded the first-year data (1992) of ECCO and took 1993 as the baseline year. The zonally integrated OHC was calculated for three periods: 1993–2005; 2006–2017; and 1993–2017. Taking into account these three periods was to identify possible shift caused by transition from ship-based observations to Argo floats (Cheng and Zhu, 2014). To some degree, this is also similar to Desbruyères et al. (2016), in which pre-2000, post-2000 and the long-term were considered.

$$\mathrm{OHC} = \rho \delta v C_p (\theta - \theta_{1993}) = \rho \delta v C_p \Delta\theta, \quad (1)$$

where ρ (kg·m^{-3}) is the seawater density, δv (m^3) is the grid volume, C_p (J·kg^{-1}·°C^{-1}) the specific heat of seawater at constant pressure, θ (°C) the annual-mean potential temperature, and θ_{1993} the annual-mean potential temperature in 1993. A value of 4.1×10^6 J·m^{-3}·°C^{-1} was used for the product of ρ and C_p (Palmer et al., 2011).

The volume-averaged potential temperature was also calculated at each depth. Additionally, we generated a detailed spatial distribution of cooling/warming trend by first calculating the vertically averaged potential temperature at each geographic location, then fitting a least-squares straight line. The linear trend was calculated using the multiple linear regression using least squares, and we used the 95% confidence level.

Heat budget analysis. Diagnostics from ECCO were used to perform a heat-budget analysis (boundaries shown in Fig. 1a). The advection calculations include the Eulerian mean and the eddy-induced parts (Forget et al. 2015; Liang et al. 2015). The vertical heat diffusion consists of isopycnal mesoscale eddy mixing (via the Redi scheme (Redi 1982)), the background diffusion, the part parametrized by the GGL90 (Gaspar et al. 1990) TKE (turbulence kinematic energy) mixing scheme, and diffusion generated by convective instability. A constant geothermal flux was also included. The heat conservation equation in ECCO is as follows (Forget et al., 2015; Piecuch, 2017).

$$\frac{\partial(s^*\theta)}{\partial t} = -\nabla_{z^*}(s^*\theta\mathbf{v}_{res}) - \frac{\partial(\theta w_{res})}{\partial z^*} + s^*\mathcal{F}_\theta + s^*D_\theta, \quad (2)$$

where s^* is a scale factor; θ is potential temperature; t is the time; $\mathbf{v}_{res} = (u_{res}, v_{res})$ and w_{res} are the total horizontal and vertical velocities, respectively; $\mathcal{F}_\theta$ is the total local forcing by surface heat exchanges (including the geothermal heating at the bottom), with shortwave radiation exponentially penetrated to a depth of 200 m (Forget et al., 2015); and D_θ is the diffusive mixing of heat. The term on the LHS (left hand side) is the total tendency; the first term on the RHS (right hand side) is the horizontal heat advection; the second term on the RHS is the vertical heat advection.

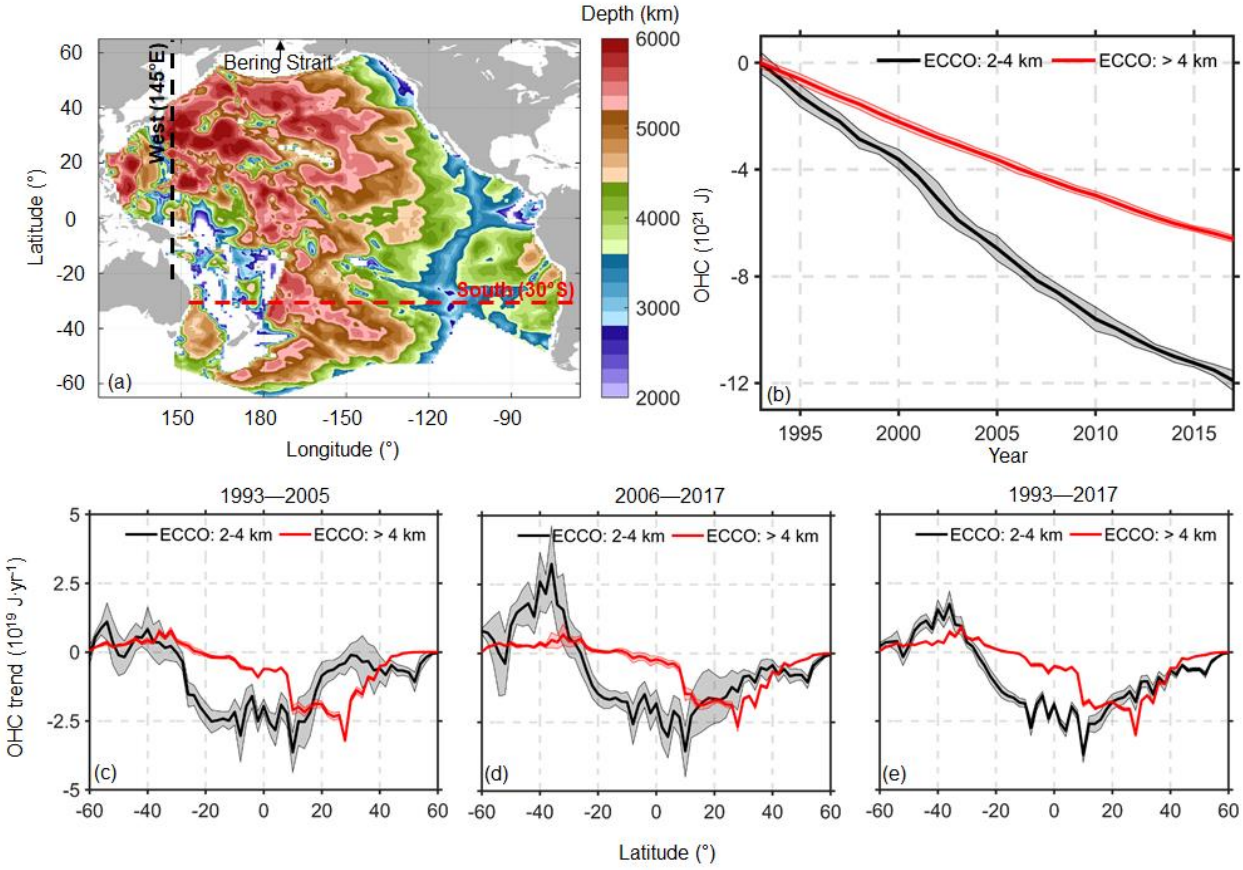

FIG. 1. (**a**) Bathymetry (>2 km), (**b**) time evolution of OHC and (**c–e**) the meridional distribution of zonal-integrated (in bins of 2°) OHC trend in the deep (2–4 km, black line) and abyssal (>4 km, red line) Pacific Oceans calculated using ECCO, with the uncertainty of ±2σ (σ: standard deviation) interval shown in shading. Similar results from the GECCO3 were shown in Fig. S1–2.

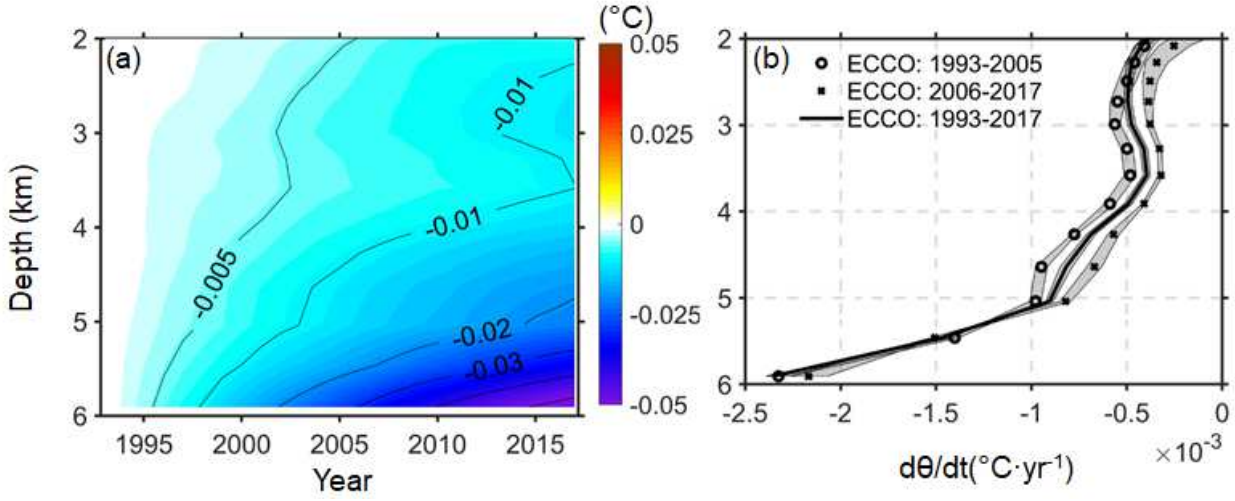

521

522 **FIG. 2.** (**a**) Potential temperature change (relative to 1993) below 2 km in the Pacific Ocean
523 from ECCO and (**b**) vertical profile of horizontally-averaged potential temperature trend. In
524 (**a**), The contour interval was 0.01 °C for values smaller than -0.01°C, and an additional interval
525 of -0.005°C also applied. In (**b**), the shading represents the 95% confidence interval. The
526 domain for this calculation can be found in Fig. 1a. Similar result from the GECCO3 was
527 shown in Fig. S3.

528

529

530

531

532

533

534

535

536

537

538

539

540

541

542

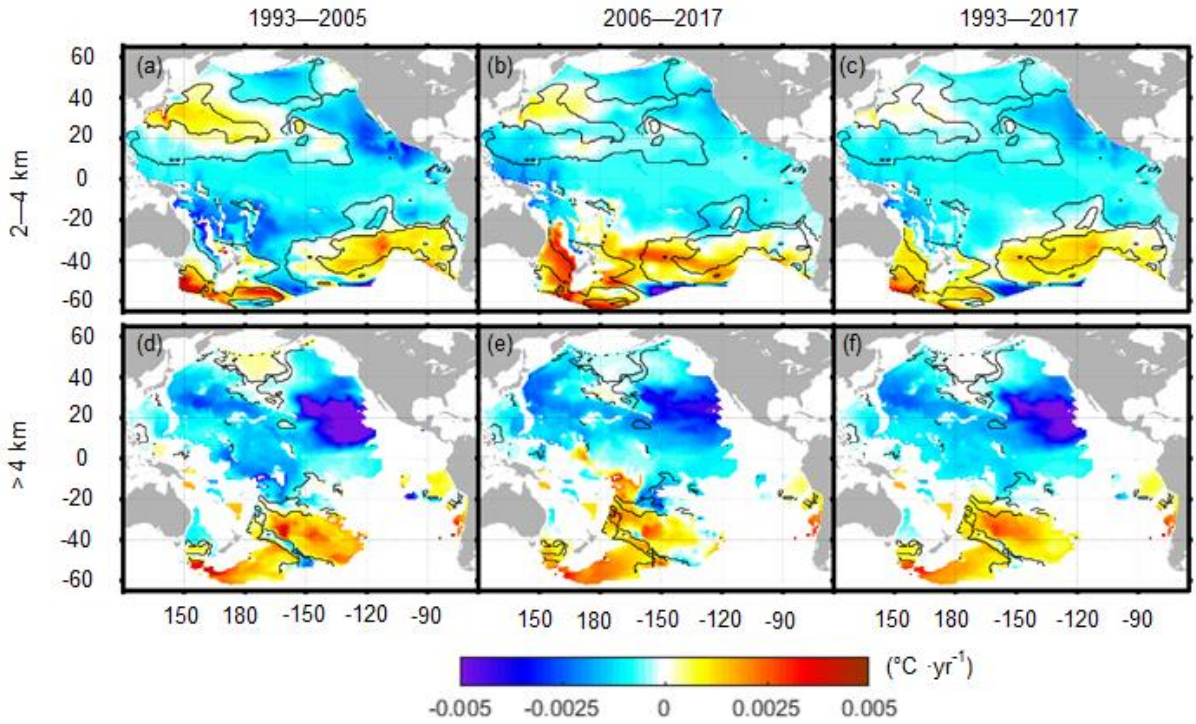

FIG. 3. Spatial distribution of linear trend of the vertically-averaged potential temperature change based on ECCO. **Top row**: deep Pacific Ocean (2–4 km); **bottom row**: abyssal Pacific Ocean (>4 km). **Left to right**: linear trend calculated over the period from 1993 to 2005, from 2006 to 2017 and from 1993 to 2017. The black contour encloses the patches where the warming or cooling is statistically significant. Similar result from the GECCO3 was shown in Fig. S4.

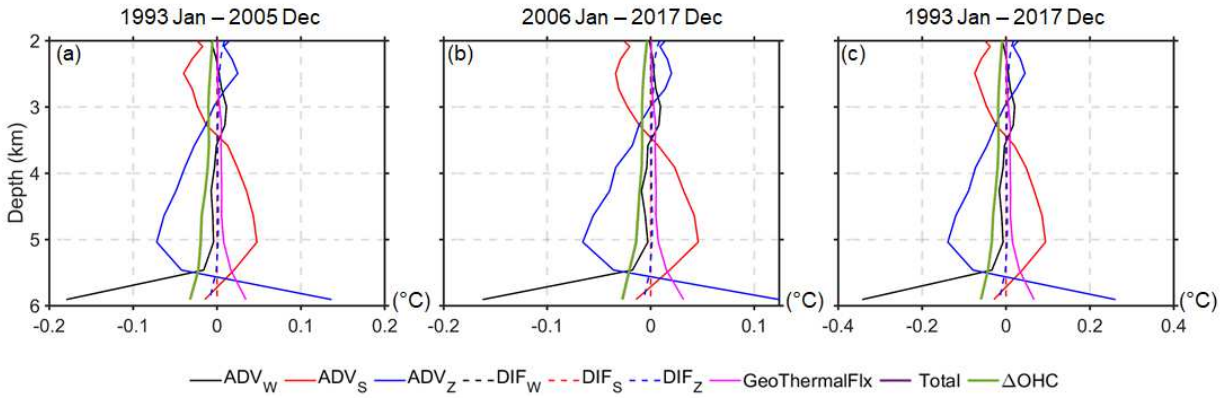

562

563 **FIG. 4.** Heat-budget analysis (total potential temperature change and its component) for the
564 Pacific Ocean below 2km based on ECCO. ADV: advection; DIF: diffusion. Subscripts: W
565 western boundary; S southern boundary; Z vertical direction. Total is a combination of all the
566 advection and diffusion processes, and the time-invariant geothermal heat flux. The purple
567 (total) and green (ΔOHC) lines almost coincide with each other, showing heat budget closure.

568

Supplementary Files

This is a list of supplementary files associated with this preprint. Click to download.

- SupLiaoetal.2022.pdf